Contents lists available at ScienceDirect

Biomaterials

Substrate stiffness and VE-cadherin mechano-transduction coordinate to regulate endothelial monolayer integrity

Roberto C. Andresen Eguiluz [a], Kerim B. Kaylan [b], Gregory H. Underhill [b], Deborah E. Leckband [a, b, c, *]

[a] Department of Chemical and Biomolecular Engineering, University of Illinois at Urbana-Champaign, Urbana, IL 61801, United States
[b] Department of Bioengineering, University of Illinois at Urbana-Champaign, Urbana, IL 61801, United States
[c] Carl R. Woese Institute for Genomic Biology, University of Illinois at Urbana-Champaign, Urbana, IL 61801, United States

ARTICLE INFO

ABSTRACT

The vascular endothelium is subject to diverse mechanical cues that regulate vascular endothelial barrier function. In addition to rigidity sensing through integrin adhesions, mechanical perturbations such as changes in fluid shear stress can also activate force transduction signals at intercellular junctions. This study investigated how extracellular matrix rigidity and intercellular force transduction, activated by vascular endothelial cadherin, coordinate to regulate the integrity of endothelial monolayers. Studies used complementary mechanical measurements of endothelial monolayers grown on patterned substrates of variable stiffness. Specifically perturbing VE-cadherin receptors activated intercellular force transduction signals that increased integrin-dependent cell contractility and disrupted cell-cell and cell-matrix adhesions. Further investigations of the impact of substrate rigidity on force transduction signaling demonstrated how cells integrate extracellular mechanics cues and intercellular force transduction signals, to regulate endothelial integrity and global tissue mechanics. VE-cadherin specific signaling increased focal adhesion remodeling and cell contractility, while sustaining the overall mechanical equilibrium at the mesoscale. Conversely, increased substrate rigidity exacerbates the disruptive effects of intercellular force transduction signals, by increasing heterogeneity in monolayer stress distributions. The results provide new insights into how substrate stiffness and intercellular force transduction coordinate to regulate endothelial monolayer integrity.

© 2017 Elsevier Ltd. All rights reserved.

1. Introduction

The vasculature is a mechanically active environment. The endothelial lining is subject to a range of mechanical perturbations such as fluid shear stress and cyclic stretch associated with respiration. The endothelium experiences a variety of endogenous and exogenous chemo-mechanical inputs that finely tune vascular homeostasis. These inputs include cell-cell and cell-substrate interactions (*e.g.* via cadherins and integrins, respectively), soluble factors (*e.g.* thrombin, nitric oxide), and mechanical factors (*e.g.* blood flow, cyclic stretch). Exogenous mechanical forces such as fluid shear stress and the stiffness of the lamina intima also regulate vascular function [1–4], and promote extracellular matrix

(ECM) deposition and cross linking [5]. *In vitro*, physiological cyclic strain further coordinates with matrix stiffness to protect endothelial junctions against disruption by vasoactive agents such as thrombin [3,4,6].

The balance between cell contractility and tethering (adhesive) forces is postulated to regulate endothelial barrier function [7,8]. This predicts that increased intercellular tension, due to elevated endogenous contractile forces, for example, would increase vascular leakage. An alternative view based on traction force microscopy measurements, is that force instability, rather than the force magnitude, predicts sites of endothelial disruption and gap formation [9]. Several factors regulate intercellular tension, such as matrix rigidity, cell contractility, and cytokines [8,10,11]. Perturbations to any of these inputs correlates with pathological responses, such as hypertension [12,13] and atherosclerosis [14]. Intimal stiffening due to age related atherosclerosis [15] or collagen over-secretion and crosslinking [16] also correlate with leaky vessels *in vivo* [17].

Force fluctuations at cell-cell contacts activate signals that increase cell contractility and regulate vascular functions [10]. Fluid shear alignment (flow sensing), for example, involves force transduction complexes at interendothelial junctions that require platelet endothelial cell adhesion molecule one (PECAM-1), vascular endothelial growth factor 2 (VEGFR2), and vascular endothelial cadherin (VE-cadherin) [1,18,19], which is the main adhesion molecule at endothelial junctions. Besides fluid shear stress, other perturbations such as cyclic stretch in the lung appear to activate a similar signaling cascade [20]. In biophysical studies, we showed that directly perturbing VE-cadherin receptors on cell surfaces with VE-cadherin-modified magnetic beads activated similar signals as in flow sensing, but without PECAM-1 [21]. We further demonstrated that VE-cadherin-activated signals increase cell contractility, disrupt peripheral junctions, and even propagate mechanical perturbations 2—3 cell diameters from the stimulated cell [21]. Thus, force transduction signals at cell-cell junctions not only induce cytoskeletal remodeling, as during shear alignment [22], but they can also disrupt endothelial monolayer integrity.

Studies demonstrated that interendothelial force transduction triggers a kinase cascade that activates integrins at the basal plane [1]. Integrins in turn increase cell contractility through the Rho/ROCK associated protein kinase pathway [23], and are well known to increase cell contractility with increasing matrix rigidity [24]. Given the coordination between cadherin force-transduction and integrins [11,25—27], we reasoned that mechanically sensitive endothelial processes that involve intercellular adhesions might also depend on substrate rigidity. Such information could enhance our understanding of the interplay between tissue mechanics and endothelial responses to perturbations that alter force at cell-cell contacts.

This study investigated the cooperation between intercellular force transduction signaling and substrate rigidity in regulating endothelial mechanics and monolayer integrity. Magnetic twisting cytometry was used to specifically activate VE-cadherin-mediated (intercellular) force transduction signals. In order to regulate the matrix rigidity, studies used micro-patterned substrates of variable, physiologically relevant stiffness. Mechanical measurements quantified the mechanical state of endothelial monolayers, and evaluated force-dependent, spatial and temporal changes in endothelial gap formation (disruption), cell tractions, and intercellular stress distributions. Our findings provide a detailed picture of the endothelial monolayer as a mechanically integrated mesoscale network. They further demonstrate how substrate rigidity modulates the impact of intercellular force transduction signaling on endothelial integrity.

2. Materials and methods

2.1. Preparation of polyacrylamide hydrogels

Polyacrylamyde (pAA) substrates were prepared following previously published protocols [8,28,29]. First, 35 mm glass bottom dishes with 13 mm wells (Cell E&G, San Diego, CA) were treated with 200 μl of 0.1 M NaOH, rinsed with distilled, deionized (DI) water, and left to dry overnight. Next, dishes were treated with amino-propyl-trimethoxysilane (Sigma-Aldrich, St. Louis, MO) for 6 min at room temperature and then rinsed exhaustively with DI water. After removing excess water, each dish was treated with 0.5% v/v glutaraldehyde in PBS for 30 min, thoroughly rinsed with DI water, and then left to dry for at least 30 min. Solutions of acrylamide and bis-acrylamide (Bis) (Bio Rad, Hercules, CA) were diluted in DI water over a range of dilutions to yield the desired gel stiffness (1.1 kPa: 7.5% acrylamide and 5% Bis; 40 kPa: 20% acrylamide and 24% Bis). pAA gels prepared for traction force microscopy (TFM)

contained a 1:1000 dilution of 0.5 μm diameter fluorescent beads (Invitrogen, Eugene, OR) as fiducial markers (see below for traction measurements). Polymerization of gel mixtures was catalyzed with 5 μl of 0.1% w/v ammonium persulfate (Bio-Rad, Hercules, CA) and 0.5 μl of $1\times$ N,N,N-tetramethylethylenediamine (Bio-Rad, Hercules, CA) for every 1000 μl of gel mixture. Next, 20 μl of the resulting mixture was placed at the center of each dish and covered with a 12 mm glass cover slip (Electron Microscopy Sciences, Hatfield, PA). The dishes were inverted during polymerization to allow bead migration to the upper surface of the gel. After polymerization, gels were immersed in 2 ml of 0.1 M HEPES buffer at pH 7 overnight at room temperature to facilitate removal of the coverslip.

2.2. Hydrogel surface functionalization

pAA substrates were covalently modified with fibronectin (FN) (human plasma, Sigma-Aldrich, F2006). To immobilize the protein, gels were activated by adding 200 μl of sulfosuccinimidyl 6-(4'-azido-2'-nitrophenylamino)hexanoate (from a stock 25 mg/ml in dimethyl sulfoxide and diluted to 1 mg/ml in 0.1 M HEPES buffer), exposed to UV light for 8 min twice, and rinsed with HEPES buffer. Once dried, protein solution at 0.1 mg/ml was incubated overnight at 4 °C and sterilized with 30 min UV light (4.5 mW/cm^2) and immersion in $1\times$ phosphate buffered saline (PBS).

2.3. Protein microarray fabrication

Protein microarrays were fabricated as previously described [30,32]. Briefly, human FN or human collagen IV (Col-IV) (EMD Millipore, CC076), both present in the tunica intima [33] was diluted to 250 μg/ml in an equal volume of $2\times$ ECM protein buffer (38% v/v glycerol in DI water, 16.4 mg/ml sodium acetate, 3.72 mg/ml EDTA, 0.5% v/v Triton X-100, ~80 μl glacial acetic acid, pH = 4.8) and pipetted into a 384-well V-bottom microplate (USA Scientific, Ocala, FL). A robotic benchtop microarrayer (OmniGrid Micro, Digilab, Marlborough, MA) was loaded with a solid pin (ArrayIt, Sunnyvale, CA; SSP015, 375 μm diameter) and used to transfer ECM solutions from the source microplate to the hydrogel substrate. Fabricated arrays were initially stored overnight at room temperature and 65% relative humidity and then subsequently at room temperature in a styrofoam container for 2 days. Before addition of cells, arrays were sterilized with 30 min UV light (4.5 mW/cm^2) and immersion in $1\times$ PBS.

2.4. Cell culture

Human pulmonary artery endothelial cells (HPAECs) (Lonza, Allendale, NJ) at passages 5—9 were cultured in T25 plastic flasks with EGM-2 culture medium (Lonza, Allendale, NJ) supplemented with 10% fetal bovine serum (FBS). Cells were harvested by treatment with 500 μl TrypLE (Gibco, Denmark) for 3 min and resuspended in 2 ml EGM-2 culture medium. Next, ~25×10^3 cells were plated on each of the previously arrayed FN or Col-IV spots on the gel surfaces. For magnetic twisting cytometry (MTC), $50-60 \times 10^3$ cells were plated on hydrogels that were coated uniformly with FN or Col-IV. After 1 h, 2 ml of EGM-2 medium was added to each dish and cells were cultured for 48 h for FN and 12 h for Col-IV at 37 °C under 5% CO_2.

2.5. Magnetic twisting cytometry (MTC)

Magnetic twisting cytometry (MTC) was used to mechanically perturb VE-cadherin receptors on the apical surfaces of HPAECs [21,34,35]. First, carboxyl ferromagnetic beads 4.5 μm in diameter (Spherotech, Lake Forest, IL) were covalently functionalized with

VE-cadherin-Fc. Beads were chemically activated with 10 mg/ml of 1-ethyl-3-(3-dimethylaminopropyl) carbodiimide hydrochloride (Sigma-Aldrich, St. Louis, MO) and 10 mg/ml N-hydroxysuccinimide (Thermo Scientific, Rockford, IL) in 1 ml 2-(N-morpholino)ethane-sulfonic acid buffer (50 mM MES, 100 mM NaCl) on an orbital shaker at room temperature for 15 min. Next, beads were centrifuged at 12,000 g for 10 min at room temperature. The supernatant was carefully aspirated, and the beads were resuspended in coupling buffer (20 mM HEPES, 100 mM NaCl, 5 mM $CaCl_2$) containing 20 μg of soluble, recombinant VE-cadherin extracellular domain or blocking anti VE-cadherin antibody (clone 75, BD Transduction Laboratories) for 2 h at 4 °C in an orbital shaker. The reaction was stopped by adding 60 μl of a quenching buffer (3.3 mM Tris-HCl, 100 mM NaCl, 5 mM $CaCl_2$). The samples were mixed for 30 min on an orbital shaker at room temperature. Again, functionalized beads were centrifuged at 10,000 g for 10 min at room temperature, and supernatant was removed by gentle aspiration. Finally, beads were resuspended in 1000 μl EGM-2 serum free medium for MTC experiments, to prevent non-specific serum adsorption to beads, yielding a final concentration of ~4×10^6–6×10^6 beads/ml. Prior to attaching the beads to the cell surface, cells were briefly serum starved for 30 min, in order to prevent serum adsorption to beads during cell binding. Then, beads were added to the cells and left to adhere to the apical surface of the cell monolayer by adding 100 μl of the modified bead solution for 20 min at 37 °C. Dishes were rinsed once with PBS to remove unbound beads, and 2 ml of EGM-2 serum free media was added. Then, dishes were placed between magnetic coils of the MTC on a heated enclosure at 37 °C. Beads were magnetized parallel to the cell monolayer by applying a magnetic field pulse (M) of 1 T for less than 0.1 ms. An oscillating magnetic field (H) with a frequency of 0.3 Hz and amplitude of 60 Gauss was then applied for 2 min, perpendicular to the cell monolayer. The oscillating field generates a twisting torque (τ) of ~7.2 Pa (Fig. 1A). The resulting displacement amplitude was a measure of the viscoelastic response of the bead-EC junction [34,35]. A displacement amplitude decay indicated a rigidity increase of the bead-EC junction (see Materials and Methods for perturbation parameters).

2.6. Thrombin perturbations

As a control, thrombin was used to induce EC contractility [8,36]. Human α-thrombin (Enzyme Research Laboratories, South Bend, IN) was added at t = 0 min to a final concentration of 0.1 U/ml, and

images of fiduciary beads in the gels were acquired at time points t = 0 and t = 120 s for traction force microscopy, as described below.

2.7. VE-cadherin-Fc purification

We used the full-length human VE-cadherin extracellular domain with a C-terminal Fc region human IgG (VE-369) followed by a C-370 terminal hexahistidine tag. The soluble protein was purified from the supernatants of Chinese Hamster Ovary (CHO) cells that were stably transfected with the VE-cadherin-Fc-His_6 construct, as described previously [21]. Soluble protein was harvested from a stably transfected CHO cell clone that was selected and cultured in Dulbecco's Modified Eagle Medium (DMEM) containing 10% v/v FBS and 800 μg/ml G418 (VWR International, Randor, PA). The soluble VE-cadherin-Fc-His_6 protein (VE-Cadherin-Fc) was affinity purified using a Ni-NTA column (Qiagen, Hilden, Germany), followed by a Protein-A Affi-Gel column (Bio-Rad, 377 Hercules, CA). Protein purity was assessed by SDS-PAGE.

2.8. Traction force microscopy (TFM)

Traction stresses in cell arrays were calculated using particle imaging velocimetry (PIV) and constraint fast Fourier traction microscopy [28]. The displacement field was obtained by comparing positions of embedded fluorescent beads, 0.5 μm in diameter, captured during the experiment to a reference image that was acquired at the end of the experiment, by detaching cells from the substrate with 1% w/v sodium dodecyl sulfate (SDS) (Thermo Scientific, Rockford, IL). The boundary of the cell array was manually traced by using the phase contrast image that was obtained at the beginning of the experiment. From bead displacements and the drawn boundary, we computed the traction field, projected area, and the net contractile moment [8,28]. The reported root mean square traction (T_{RMS}) and net contractile moment (NCM) values were normalized for each sample as follows:

$$T_{RMS} = \frac{T_{RMS}^f}{T_{RMS}^0} \tag{1}$$

$$NCM = \frac{NCM^f}{NCM^0} \tag{2}$$

where T_{RMS}^0 and NCM^0 are the RMS traction and NCM calculated at
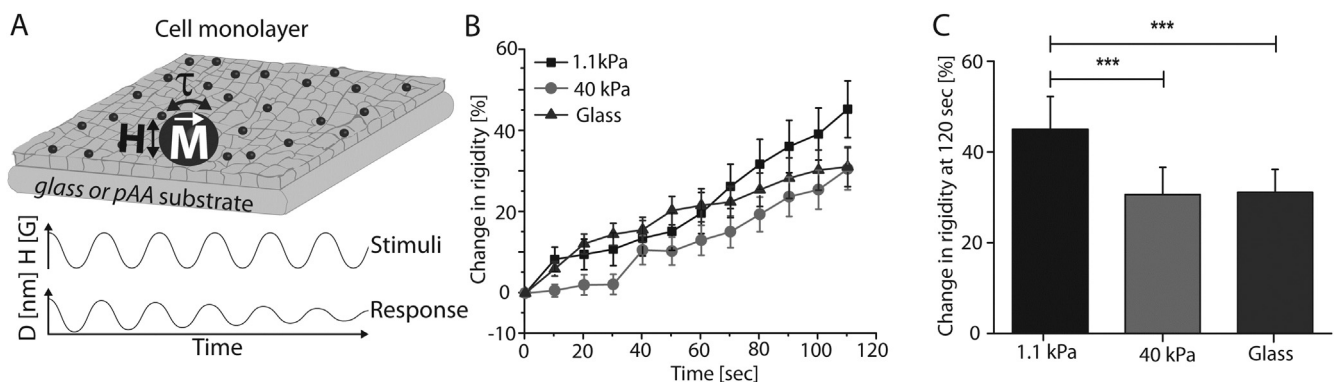

Fig. 1. **VE-cadherin mediated adaptive cell stiffening depends on substrate rigidity.** (A) Schematic of the MTC showing magnetized beads (**M**), oscillating magnetic field (**H**), and resulting twisting torque (τ) that displaces beads. Bead displacement amplitudes reveal the viscoelastic behavior of the bead-cell junction. All beads were functionalized with VE-cadherin-Fc. (B) Time dependence of force actuated percent change in the rigidity of the bead-cell junction relative to the initial basal value. Endothelial monolayers grown on soft (1.1 kPa) and stiff (40 kPa) pAA hydrogels, and glass (50 GPa, blue) substrates were perturbed with VE-cadherin coated beads for 120 s. (C) Percent change in rigidity of the bead-cell junction after a 120 s perturbation, relative to basal values. Data represents mean ± s.d. (n = 212 for glass, n = 202 for 40 kPa, and n = 181 for 1.1 kPa beads, *** $p < 0.001$).

time t = 0, and T_{RMS}^f and NCM^f were calculate at t = 120 s.

2.9. Monolayer stress microscopy (MSM)

Monolayer stress distributions were computed, by modeling the cell monolayer as a homogeneous, linearly-elastic thin plate whose internal stress field balances the traction stresses at the basal plane of the cell monolayer (Figs. 5 and 6) [37]. In order to calculate the traction stresses, we first defined the substrate strain field, which is then imposed on the thin-plate to yield an invariant solution to the material properties of the thin plate—that is, the elastic properties of the thin-plate (cell monolayer) are not required to calculate the stress distribution [38,39]. In order to compute the monolayer stresses, the monolayer thickness (h) was measured by confocal imaging of fixed immunostained samples and found to be h = 5 μm. Manually traced cell array boundaries used to calculate cell tractions were in turn used for MSM calculations. The average normal (σ_{ave}) and average shear (μ_{ave}) stresses were computed from the maximum and minimum principal stresses, σ_{max} and σ_{min} as follows:

$$\sigma_{ave} = \frac{\sigma_{max} + \sigma_{min}}{2} \tag{3}$$

$$\mu_{ave} = \frac{\sigma_{max} - \sigma_{min}}{2} \tag{4}$$

σ_{ave} and μ_{ave} were then normalized for each sample as follows:

$$\sigma_{norm} = \frac{\sigma_{ave}^f}{\sigma_{ave}^0} \tag{5}$$

$$\mu_{norm} = \frac{\mu_{ave}^f}{\mu_{ave}^0} \tag{6}$$

where σ_{ave}^0 and μ_{ave}^0 are the at root mean square values of σ_{ave} and μ_{ave} at time t = 0 s and σ_{ave}^f and μ_{ave}^f at time t = 120 s. σ_{max} histograms were plotted by first filtering all non-zero values (that is, selecting only the stress vectors within the domain) and a bin size of 1–5 Pa.

2.10. Immunochemistry and imaging

To visualize subcellular remodeling due to VE-cadherin bond shear in cells cultured on 1.1 kPa, 40 kPa, and glass substrata, cell monolayers were fixed and stained as previously described [21]. Monolayers were washed in PBS and fixed for 15 min in 4% w/v paraformaldehyde at pH 7.4. Following extensive washing with PBS, monolayers were then permeabilized with 0.1% v/v Triton-X in PBS and blocked for 20 min in 2% w/v bovine serum albumin (BSA) at pH 7.4, which we call blocking buffer. Primary antibodies, secondary antibodies, and rhodamine-phalloidin (Invitrogen, CA) were diluted in blocking buffer as follows: primary antibodies consisted of goat anti-VE-cad C19 (SC6458, Santa Cruz Technologies, Dallas, TX) at 1:50 and mouse anti-Paxillin (612405, BD Biosciences, NJ) at 1:200. Secondary antibodies or labels consisted of rabbit anti-goat-FTIC (F7367, Sigma, MO), rabbit anti-mouse 647 (A21239, Invitrogen, CA), and rhodamine-phalloidin (R415, Invitrogen, CA), all at 1:200. Diluted primary antibodies were incubated for 1 h, followed by thorough washing. Secondary antibodies and rhodamine-phalloidin were co-stained for 1 h. Finally, after several washing steps, monolayers were mounted with Pro Long Gold Antifade Reagent (Invitrogen, CA).

Imaging was performed on a Zeiss LSM 700 laser scanning confocal microscope. Fluorescent excitation wavelengths were of 405 nm, 488 nm, 555 nm, and 633 nm. Here, 16-bit 512 × 512 images were collected using either a 20× objective (air) for quantifying the width of cell-cell junctions and interendothelial gap sizes, or a 40× and 1.3 NA objective (oil immersion) for focal adhesion (FA) analysis (see Focal adhesion analysis section).

2.11. Focal adhesion analysis

Focal adhesions were first immunostained with anti-paxillin antibody, as indicated in the Immunochemistry and imaging section. Confocal images of paxillin were analyzed with a custom MATLAB code, based on the watershed algorithm [40]. Following this analysis, FA size and count were quantified using the Analyze Particles function in ImageJ (NIH) with a minimum threshold area of 0.3 μm² [41]. FA counts were normalized per cell. The surfaces of most pAA gels are somewhat uneven such that the surface of the gel was not entirely in the focal plane. With samples presenting a significant tilt, three z-stack planes were analyzed individually by confocal microscopy. Using ImageJ, a stack was created with the analyzed images and the maximum intensities projected into one single image, which was then used to analyze the FA number and area.

2.12. Statistical analysis

All statistical analyses were performed using GraphPad Prism 5 (GraphPad Software, La Jolla, CA). All data are presented as the mean ± standard error of the mean. Two-tailed Student's t-tests were used to compare two quantities and p-values <0.05 were considered statistically significant.

3. Results

3.1. VE-cadherin activated cell stiffening depends on substrate stiffness

VE-cadherin complexes transduce intercellular forces to activate cytoskeletal remodeling [42], as well as signaling cascades that increase cell contractility [10,21]. The increased contractility in turn both increased traction force generation in single cells [26] and destabilized peripheral cell-cell junctions in endothelial monolayers, resulting in increased intercellular gap formation [21]. Here we investigated how substrate stiffness, which regulates the cell pre-stress—that is, the intrinsic cell contractility [43]—affects the force-activated, VE-cadherin-mediated stiffening of human pulmonary artery endothelial cells (HPAECs). We used VE-cadherin modified magnetic beads to perturb VE-cadherin receptors at the apical surfaces of ECs cultured on soft (1.1 kPa) and stiff (40 kPa) hydrogels, or on glass (~50 GPa).

Magnetic twisting cytometry (MTC) [21] (Fig. 1A) was used to mechanically stimulate VE-cadherin receptors on endothelial cells (EC). We previously reported that force-loading cadherin receptors activated cell stiffening [43], but here we showed that the amplitude of the stiffening response depends on substrate rigidity (Fig. 1B). With monolayers on soft hydrogels (1.1 kPa), the cell stiffness increased by 45 ± 7%, relative to the basal stiffness, after 120 s of force-loading. This change was higher than the 31 ± 6% and 31 ± 5% relative stiffening measured with cells on stiff hydrogels (40 kPa) or on glass, respectively (Fig. 1C). The difference between the stiffening responses of cells on soft versus rigid substrates was statistically significant, at the 95% confidence level ($p < 0.001$, $n > 180$ bead-cell junctions). Cells seeded on Col-IV also exhibited adaptive stiffening when cultured on stiff gels (40 kPa) and on glass (~50 GPa) (S.I.1).

3.2. Increased tension between cells on rigid substrates remodels intercellular junctions and increases gap formation in mechanically perturbed monolayers

Both substrate stiffness [8,36] and force-activated mechano-transduction signals [21] affect cell junction integrity and trigger junction remodeling [10,44,45]. Here, we investigated their combined effect on the morphology of junctions between cells in mechanically stimulated EC monolayers. After perturbing VE-cadherin receptors for 120 s with VE-cadherin coated ferromagnetic beads (Fig. 2A), we quantified the contact areas between cells on soft versus rigid substrates, relative to unperturbed cells. The average contact area between unperturbed cells on soft 1.1 kPa gels (218 ± 11 μm^2) was 29% larger than between ECs on 40 kPa hydrogels (168 ± 5.5 μm^2), and 22% greater than junctions between cells on glass (178 ± 8 μm^2). Following VE-cadherin force-loading, the average contact area between ECs on soft hydrogels appeared to decrease slightly to 194 ± 16 μm^2, but the difference was not statistically significant ($p = 0.27$, $n > 100$ cells). The junction areas were still 32% larger than junctions between mechanically perturbed cells on glass (147 ± 7 μm^2). Only ECs on glass exhibited a significant 18% decrease in intercellular contact area, with the
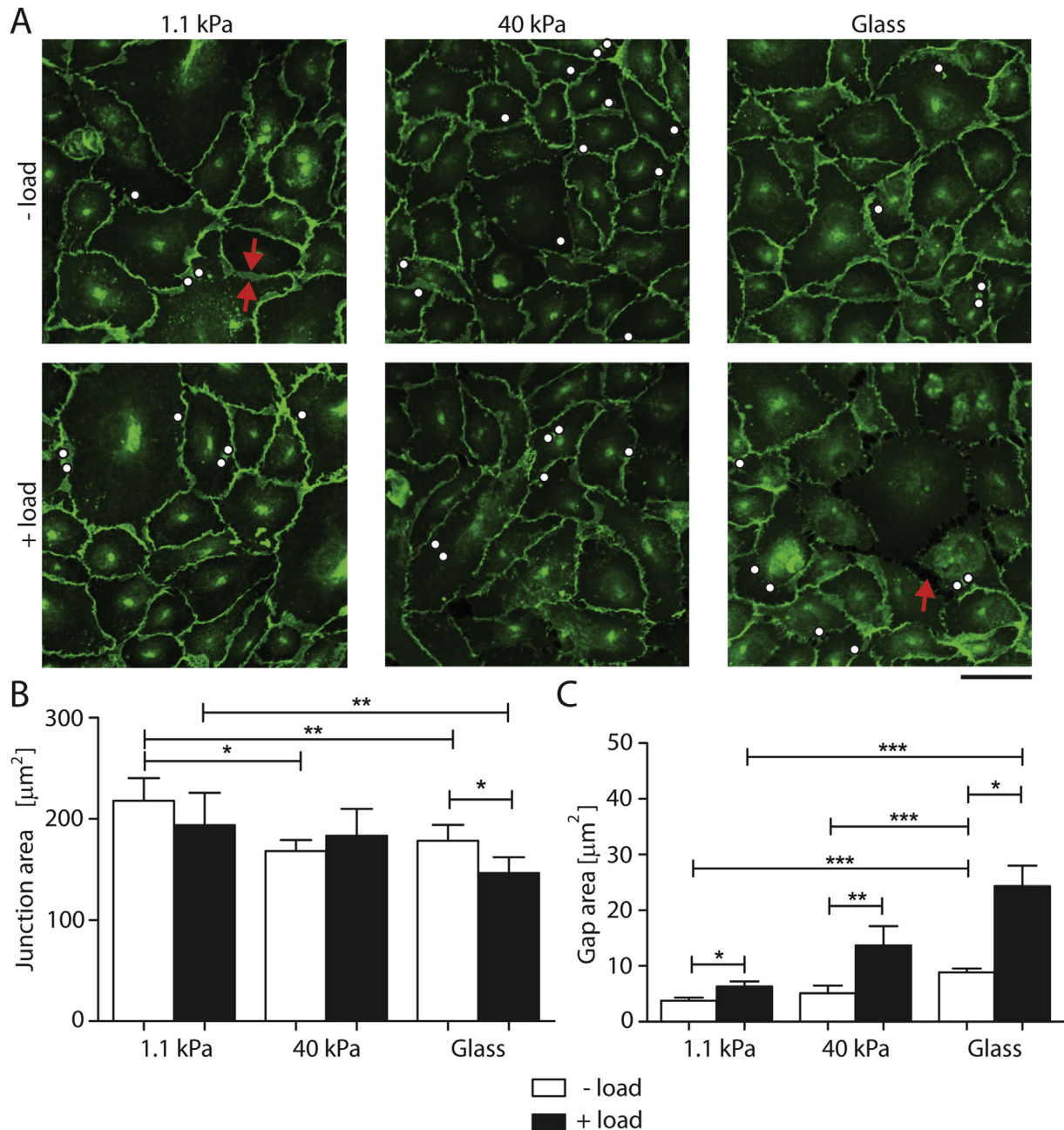

Fig. 2. Substrate stiffness modulates intercellular junction remodeling following VE-cadherin-mediated mechanotransduction. (A) Confocal immunofluorescence images of EC monolayers bound with VE-cad-Fc beads without (−load) and with (+load) applied perturbation. Scale bar = 50 μm. The immunofluorescence images show VE-cadherin distributions on 1.1 kPa, 40 kPa, and glass (~50 GPa) substrata. White dots indicate locations of VE-cadherin coated beads. Red arrows show junction area and gap. Images represent >10 images per condition from 3 independent experiments. (B) and (C) Quantification of interendothelial junction and gap areas between endothelial cells without and with oscillating shear stress for 120 s ($n = 100–150$ cells from 3 independent experiments). Data show the mean ± s.e.m. * $p < 0.05$, ** $p < 0.01$, *** $p < 0.001$. (For interpretation of the references to colour in this figure legend, the reader is referred to the web version of this article.)

average area decreasing from 178 ± 8 μm^2 to 147 ± 7 μm^2, following VE-cadherin mechanotransduction ($p = 0.03$, $n = 120$ cells) (Fig. 2B). The average intercellular contact areas under different conditions are summarized in Supplemental Table 1.

To further characterize force-activated interendothelial junction remodeling, we measured the areas of intercellular gaps in monolayers on soft (1.1 kPa) and on stiff (40 kPa) hydrogels, and on glass (~50 GPa). Even without VE-cadherin specific perturbations (−load), there were some gaps in all monolayers. The average measured gap area on soft hydrogels (3.8 ± 0.6 μm^2) was more than 2-fold smaller than between cells on glass ($8.9 \pm$ μm^2; $p = 0.0004$, $n = 120-450$ gaps), but not statistically different from cells on 40 kPa gels (5 ± 1 μm^2; $p = 0.3$, $n = 50-120$). This behavior was qualitatively similar to a prior report [8].

Force loading VE-cadherin receptors (+load) triggered an increase in the gap area in monolayers on all substrates investigated, but the increases were greater on stiff substrates. On soft hydrogels, the gap area increased 67% from 3.8 ± 0.6 μm^2 to 6.3 ± 0.9 μm^2, while the average gap area increased 170% (from 5 ± 1 μm^2 to 14 ± 4 μm^2), and 175% (from 8.9 ± 0.7 μm^2 vs 24 ± 4 μm^2) on, respectively, stiff hydrogels and glass (Fig. 2C). The results obtained with ECs cultured on glass are similar to a prior report [21]. The measured average gap areas are summarized in Table 1.

3.3. Force loading VE-cadherin receptors triggers cell-matrix junction remodeling

VE-cadherin and integrins are both involved in the mechano-sensing in cells [46], and they are linked through common signaling pathways that regulate cell contractility and the distribution of tension between intercellular and cell-matrix adhesions [26,47—49]. Recent findings demonstrated that signals activated by force loading E-cadherin in epithelia and PECAM-1 in endothelia trigger the downstream formation of new integrin adhesions in single cells on relatively stiff hydrogels (34 kPa) or on glass [26,49]. Here we tested whether substrate rigidity affects FA remodeling triggered by VE-cadherin force transduction in confluent EC monolayers. Using paxillin as a marker for integrin-based FA (Fig. 3A), we quantified the FA number/cell (Fig. 3B) and the average FA area (Fig. 3C) before and after VE-cadherin force loading. After VE-cadherin specific perturbations (+load), FA numbers increased in cells cultured on rigid substrates. On soft hydrogels (1.1 kPa) the slight increase in FA number from 13 ± 2 to 15 ± 4 FAs per cell was not significant ($p = 0.69$, $n = 80-100$ cells). On stiff hydrogels (40 kPa) and on glass, force loading VE-cadherin receptors triggered statistically significant increases in the FA numbers, relative to unperturbed cells. The number per cell increased from 19 ± 1 to 25 ± 2 (34%; $p = 0.009$, $n = 70-75$ cells) and from 14 ± 2 to 23 ± 1 (62%; $p = 0.002$, $n = 70-80$ cells) when cells were cultured on stiff gels (40 kPa) and on glass, respectively. There were also more FAs per cell on stiff (40 kPa) than on soft (1.1 kPa) hydrogels, prior to VE-cadherin force loading (−load): there were 42% more FAs on stiff hydrogels (13 ± 2 per cell) relative to soft gels (19 ± 1 per cell) ($p = 0.012$, $n = 80$ cells) (Fig. 3B).

Force-loading VE-cadherin receptors also triggered an increase in the average FA size. On soft hydrogels (1.1 kPa), the average FA

size did not change significantly: the apparent difference between 0.57 ± 0.03 μm^2 and 0.5 ± 0.01 μm^2 was not significant ($p = 0.227$, $n = 80-100$ cells). In cells on stiff hydrogels (40 kPa) and on glass, upon VE-cadherin force loading, the FA size increased 32% (from 0.7 ± 0.02 μm^2 to 0.9 ± 0.1 μm^2; $p = 0.037$, $n = 70-75$ cells) and 47% (from 0.6 ± 0.02 μm^2 to 0.9 ± 0.1 μm^2; $p = 0.044$, $n = 70-80$ cells), respectively. Interestingly, in the absence of VE-cadherin perturbations, but with bound VE-cadherin-coated beads, the FAs were largest on stiff hydrogels (40 kPa), being 23% higher than those in cells on soft (1.1 kPa) hydrogels ($p = 0.002$) and 13% higher than in cells on glass ($p = 0.007$).

Similar to E-cadherin force transduction in single epithelial cells [26], these results show that VE-cadherin-specific perturbations activate downstream signals that cause FA remodeling, and confirm that substrate stiffness regulates FA size and number. Thus, although integrin activation is initiated by intracellular signals, the overall stiffening response and FA remodeling also clearly depend on the cell-prestress and on outside-in rigidity sensing.

3.4. Local, VE-cadherin force transduction signals at the cell level do not alter the mechanical balance of endothelial colonies

One postulate is that the balance between cell-matrix and cell-cell binding stresses regulate the integrity of interendothelial junctions [7,39,45], and that mechanical homeostasis requires a coordinated modulation of cell-matrix adhesion, actomyosin contractility, and cell-cell adhesion [39,45,50]. ECs may form a mechanically integrated network that dynamically redistributes and re-localizes stresses to maintain mechanical homeostasis. In prior studies of EC monolayers on glass, VE-cadherin force trans-duction signaling disrupted interendothelial junctions at distances of up to 2—3 cell diameters from the perturbed cell. To investigate how VE-cadherin-specific force transduction alters the cell-matrix and cell-cell stresses in large confined EC colonies, we combined magnetic twisting cytometry (MTC) with traction force microscopy (TFM) and monolayer stress microscopy (MSM) (Fig. 4A). We used: i) MTC to activate VE-cadherin mediated cell contractility [21], ii) TFM to recover tractions and calculate contractility of EC colonies on soft (1.1 kPa) and stiff (40 kPa) hydrogels [8], and iii) MSM to calculate the stress distribution within the EC monolayer (the EC colony) [37] (Fig. 4B).

For these studies, ECs were plated on soft (1.1 kPa) and stiff (40 kPa) hydrogels, for 48 h. First, we observed that EC colonies on stiff (40 kPa) hydrogels occupied 33.8% larger areas than those on soft hydrogels (1.1 kPa) ($189,000 \pm 9000$ μm^2 vs. $260,000 \pm 8000$ μm^2) ($p = 0.0001$, $n = 23$, Fig. 5A). Cell-cell adhe-sions reportedly allow cell spreading on more compliant substrates [51], and cells did spread on soft hydrogels. However, despite identical microarray conditions, cells were more spread on the stiffer gels. Cell densities were similar on both gels; consequently, the substrate stiffness determined the final spread area of the EC colony.

Tractions were recovered from measured fiduciary bead dis-placements (Fig. 5B—E), and monolayer stresses were computed (Fig. 6) at two time points, t = 0 and t = 120 s, with and without 120 s of VE-cadherin receptor perturbation (±load). Traction heat maps exhibited large spatial heterogeneities on both substrate stiffnesses investigated, and VE-cadherin did not significantly change the distributions (Fig. 5B). VE-cadherin-specific loading did not trigger large changes in the RMS tractions and net contractile moments (NCM) of the entire EC colonies. On soft hydrogels (1.1 kPa), the normalized RMS traction of the entire EC colony of bead-laden, unperturbed cells (−load) was 1.02 ± 0.05. The normalized RMS traction following VE-cadherin force loading (+load) was 0.93 ± 0.03, and is statistically similar to the no-load

Table 1
Measured average gap area for unperturbed and perturbed endothelial monolayers for the three investigated substrate stiffnesses.

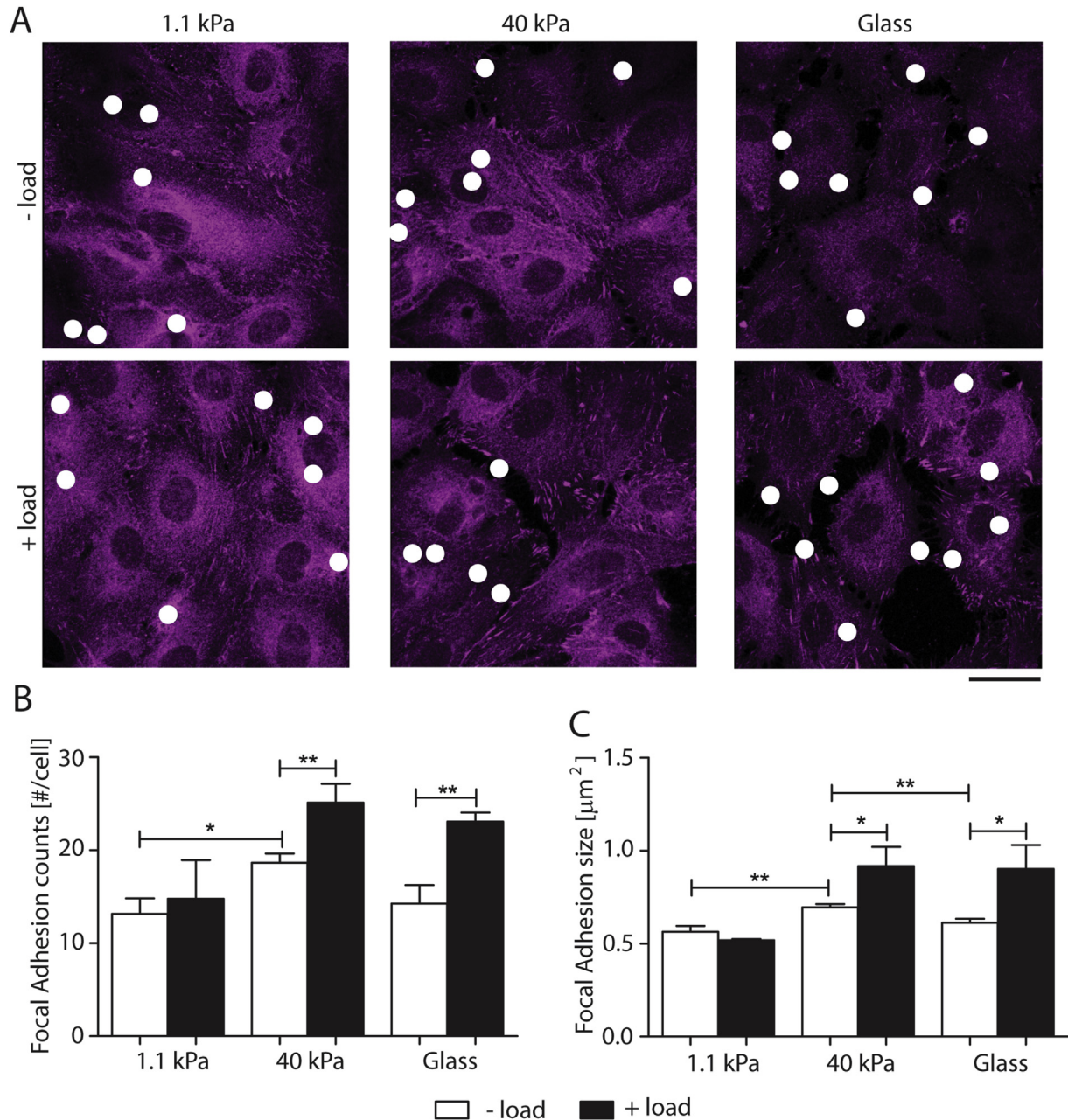| Substrate stiffness	−load [μm^2]	+load [μm^2]
1.1 kPa	3.8 ± 0.6	6.6 ± 0.9
40 kPa	5 ± 1	14 ± 4
Glass (~50 GPa)	8.9 ± 0.7	24 ± 4

Fig. 3. VE-cadherin mechanotransduction alters the number and size of focal adhesion. (A) Confocal images of immunofluorescence EC monolayers showing focal adhesions without (−load) and with (+load) VE-cadherin specific perturbations. FAs were stained for paxillin. Scale bar = 25 μm. White dots indicate the location of VE-cadherin coated beads. (B) and (C) Quantification of FA number per cell and size, respectively, without (white bars) and with (black bars) oscillating shear stress for 120 s ($n = 70-100$ cells over 2 independent experiments). Data show the mean $\pm$ s.e.m. * $p < 0.05$, ** $p < 0.01$.

condition ($p = 0.12$, $n = 10-11$ colonies) (Fig. 5C), similar trend to what observed on stiff substrates functionalized with Col-IV (0.89 ± 0.12 vs. 1.05 ± 0.18 for −load and +load, respectively, $p = 0.52$, $n = 2$)(S.I.2B). The NCM is a scalar measure of cell colony contractile strength (Fig. 5D) [28]. On soft gels, the normalized NCM of mechanically perturbed ECs was 0.99 ± 0.06, and is statistically similar to the value of 1.1 ± 0.1 determined for the unperturbed colony ($p = 0.53$, $n = 10-11$ colonies). On stiff hydrogels (40 kPa), the normalized RMS traction of EC colonies following VE-cadherin-specific perturbations was 0.88 ± 0.05, and that of the unperturbed colonies was 1.00 ± 0.04 (Fig. 5C), corresponding to a decrease of 12%, at the 95% confidence level ($p = 0.048$, $n = 10-11$). Normalized RMS tractions determined in control measurements of beads

coated with the blocking anti-VE-cadherin were statistically similar to the unperturbed bead-laden ECs (1.00 ± 0.04 vs. 0.90 ± 0.01; $p = 0.18$, $n = 10-11$). The normalized RMS traction of thrombin-stimulated EC colonies on 40 kPa gels in a positive control, was 0.98 ± 0.12, and was statistically similar to the unperturbed cells ($p = 0.35$, $n = 3-11$). The normalized NCM of 1.4 ± 0.1 determined after force loading VE-cad beads on cells on stiff hydrogels was not significantly different from that of unperturbed cells (1.8 ± 0.3; $p = 0.32$, $n = 10-11$) (Fig. 5D). Histograms of distributions of the traction magnitude, ITI, presented a positive skewness and population. VE-cadherin force loading did not shift the peaks of the distributions significantly.

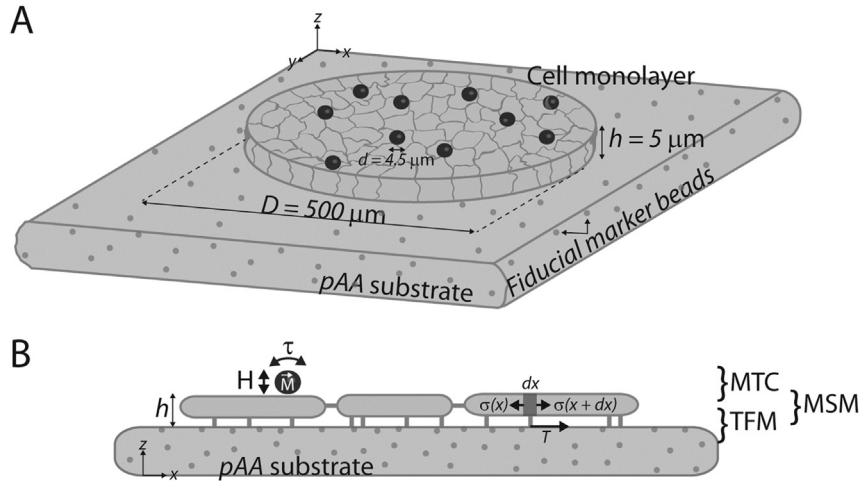Similarly, the apparent difference in the normalized NCM of

Fig. 4. Integrated platform that combines MTC, TFM, and MSM to quantify stresses due to VE-cadherin mechanotransduction in EC monolayers. (A) FN arrays 500 μm in diameter on pAA substrates with embedded fiducial marker beads were seeded with HPAECs for 48 h, yielding regular circular cell colonies with 200—280 cells and 5 μm height. (B) Schematics showing the applied stresses (MTC), recovered stresses (tractions), and calculated stresses (MSM).

1.4 ± 0.3 and 1.7 ± 0.2 determined with and without, respectively, force loading with anti-VE-cadherin coated beads was not significantly different ($p = 0.19$, $n = 10—11$ colonies). However, in the positive control, thrombin treatment triggered a dramatic increase in the normalized NCM to 7 ± 1, relative to untreated cells (1.4 ± 0.2; $p < 0.0001$, $n = 3—10$) and relative to cells perturbed with anti-VE cadherin coated beads (1.7 ± 0.2; $p < 0.0001$, $n = 3—11$).

Prior findings with ECs on glass showed that VE-cadherin force transduction activated contractility that disrupted interendothelial junctions 2—4 cell diameters from the point of stimulation [21]. To investigate how such VE-cadherin stimulated signals altered force distributions in the monolayer, we computed the average normal stress σ_{ave} and the average shear stress μ_{ave} (eqs. (5) and (6)), respectively), by imposing the determined tractions as the strain field that was used to compute the corresponding stress fields in the monolayer. To do this, we modeled the EC colony as a homogeneous thin plate. On soft hydrogels (1.1 kPa), in the absence (−load) and presence (+load) of VE-cad specific perturbations, the average normal stress in the monolayer σ_{ave} was unchanged (Fig. 6A), with calculated values being 1.03 ± 0.05 and 0.99 ± 0.11 for the unperturbed and perturbed monolayers, respectively ($p = 0.8$, $n = 11$ colonies). Changing the surface ligand from FN to Col-IV did not affect this behavior, within experimental error (0.99 ± 0.14 vs. 1.2 ± 0.07 for −load and +load, respectively, $p = 0.32$, $n = 2$) (S.I.2C). Similarly, the average intercellular shear stress μ_{ave} (Fig. 6D) of perturbed and unperturbed colonies were 1.02 ± 0.04 and 1.0 ± 0.1, respectively, and were statistically similar ($p = 0.82$, $n = 11$ colonies). We also did not observe any force-dependent changes in EC colonies on stiff hydrogels (40 kPa). Values for σ_{ave} of 1.00 ± 0.09 and 1.01 ± 0.09, for mechanically stimulated versus unperturbed cells, respectively, are similar ($p = 0.93$, $n = 9—11$ colonies). Values for μ_{ave} of perturbed and unperturbed colonies were, respectively, 0.94 ± 0.09 and 0.88 ± 0.05, and are statistically similar ($p = 0.55$, $n = 9—11$). In a positive control, thrombin treatment induced a significant increase in normalized σ_{ave} to 1.9 ± 0.4 (Fig. 6A). Values of the normal and shear stresses are summarized in Table 2.

Because the thin plate model does not consider the formation of gaps, we corrected σ_{ave} and μ_{ave} to account for the reduction in EC colony area. We corrected σ_{ave} and μ_{ave} of each condition at time points t = 120 s, taking the measured gap areas (Fig. 2C) into account for each specific condition, by applying eq. (7):

$$\sigma_{ave}^{corrected} = \frac{\sigma_{ave}}{1 - \frac{\Sigma A_{gaps}}{A_{image}}} \tag{7}$$

were $\sigma_{ave}^{corrected}$ is the corrected average stress, σ_{ave} the computed average stress considering a homogeneous thin plate, ΣA_{gaps} is the sum of the gaps per field of view, and A_{image} is the area of the field of view. We similarly corrected the average shear stress $\mu_{ave}^{corrected}$, by exchanging μ for σ. The corrected values (Fig. 6A and B and Table 2) did in fact increase the values of σ_{ave} and μ_{ave}. However, VE-cadherin perturbations did not significantly change the corrected values, relative to the no-load control.

The representative stress heat maps (σ_{max}) and average, normalized values are further validated by histograms of the stress vectors (σ_{max}) (Fig. 7). On both soft and stiff substrata, the histograms exhibited normal (Gaussian) distributions, although with cells on stiff substrata, the peaks of the histograms were at higher values and the standard deviation was larger than measured with colonies on soft gels. VE-cadherin force loading did not shift any of the distributions significantly (Fig. 7), although the standard deviation of the distribution determined with cells on stiff substrata decreased from 495 Pa to 424 Pa at t = 0 s and t = 120 s, respectively. Only thrombin treatment resulted in a significant change in the peak of the σ_{max} distribution, from 55 Pa to 532 Pa.

Signals activated by local cadherin perturbations that increase cell contractility shifted neither the normalized RMS traction nor the normalized NCM of the colonies. However, in unperturbed EC monolayers on soft versus stiff hydrogels, there were significant differences in both the shear and normal stresses (Fig. 6C and D and Fig. S1). On soft substrates, the peaks and the standard deviations of the distributions are smaller (Fig. 7, Table 1) than determined with 40 kPa gels, indicative of lower and more uniformly distributed stresses in the monolayer. The heat maps also revealed large fluctuations in the stress distributions within monolayers on rigid hydrogels. Local force transduction signals induced cell contractions and disrupted the peripheral junctions of the perturbed cells (Fig. 2C). However, in comparison with the thrombin treated cells, our results suggest that the pre-existing, large stress variations within the monolayer mask smaller, local changes caused by VE-cadherin force transduction.
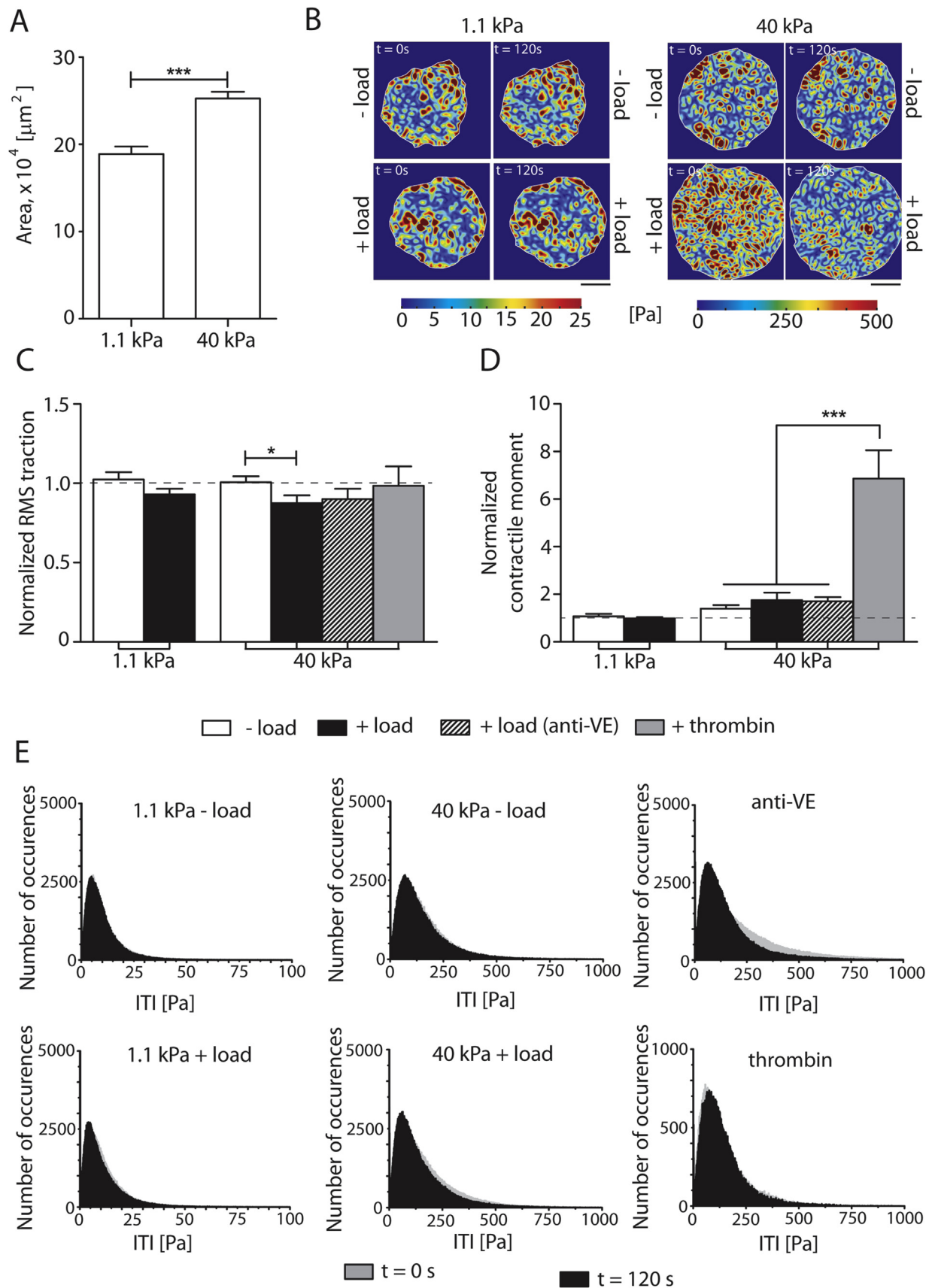
Fig. 5. Effect of VE-cadherin mechanotransduction and substrate rigidity on endothelial cell traction forces. (A) Projected area of EC colonies plated on 1.1 kPa and 40 kPa. (B) Representative heat maps showing tractions at time points t = 0 s and t = 120 s for soft and stiff hydrogels without (−load) and with force loading (+load). Scale bars = 150 μm, showing the heterogeneous spatial tractions distribution. (C) Normalized RMS traction of cell colonies. (D) Normalized NCM. (E) Frequency histograms of the tractions magnitude showing the tractions magnitude distribution, ITI at time points t = sec (grey) and t = 120 s (black). Data show the mean ± s.e.m. n = 10, 11, 10, 11, 11, and 3 for the 1.1 kPa −load, 1.1 kPa +load, 40 kPa −load, 40 kPa +load, 40 kPa +load (anti-VE), and +thrombin, respectively. *$p < 0.05$, ***$p < 0.0001$.
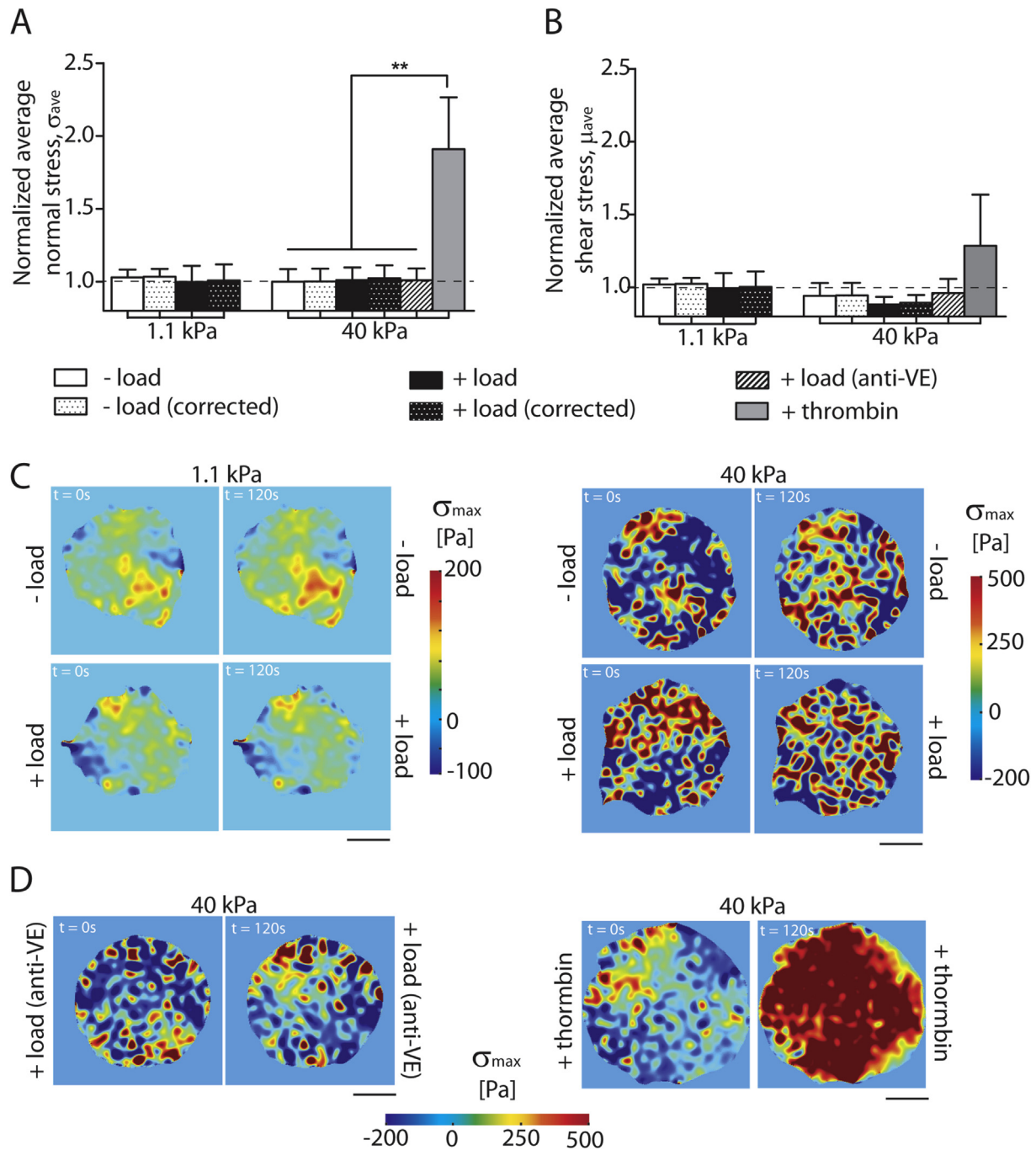
Fig. 6. Effect of VE-cadherin mechanotransduction and substrate rigidity on the distributions of the maximum stresses in the endothelial monolayers. (A) Normalized σ_{ave}, ±load and (B) normalized μ_{ave}, ±load. (C) Representative heat maps showing monolayer σ_{max} distributions at time points t = 0 s and t = 120 s for soft and stiff hydrogels. (D) Representative heat maps showing σ_{max} for same conditions as (A) for negative (anti-VE) and positive (thrombin) controls. Data show the mean ± s.e.m. n = 10, 11, 10, 11, 11, and 3 for the 1.1 kPa −load, 1.1 kPa +load, 40 kPa −load, 40 kPa +load, 40 kPa +load (anti-VE), and +thrombin, respectively. **p < 0.005.

Table 2
Computed average normal and shear stresses for the endothelial colonies for all investigated conditions. ND = not determined.

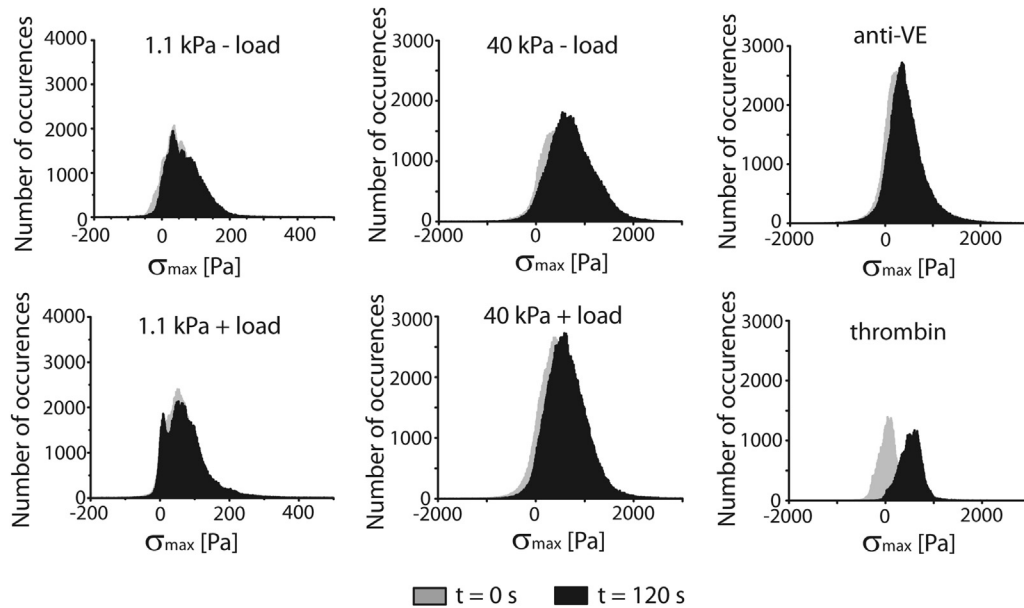| Perturbation	−load				+load				+load anti-VE		+ thrombin	
Stiffness	σ_{ave}	$\sigma_{ave}^{corrected}$	μ_{ave}	$\mu_{ave}^{corrected}$	σ_{ave}	$\sigma_{ave}^{corrected}$	μ_{ave}	$\mu_{ave}^{corrected}$	σ_{ave}	μ_{ave}	σ_{ave}	μ_{ave}
1.1 kPa	1.03 ± 0.05	1.03 ± 0.05	1.02 ± 0.04	1.02 ± 0.04	1.0 ± 0.1	1.0 ± 0.1	0.9 ± 0.1	1.0 ± 0.1	ND	ND	ND	ND
40 kPa	1.00 ± 0.09	1.00 ± 0.09	0.94 ± 0.09	0.94 ± 0.09	1.01 ± 0.09	1.03 ± 0.09	0.88 ± 0.05	0.89 ± 0.05	1.01 ± 0.08	0.96 ± 0.10	1.91 ± 0.36	1.29 ± 0.35

Fig. 7. Histograms of the maximum shear stresses determined under the indicated conditions. σ_{max} vectors at timepoints t = 0 s (grey) and t = 120 s (black). n = 10, 11, 10, 11, 11, and 3 for the 1.1 kPa −load, 1.1 kPa +load, 40 kPa −load, 40 kPa +load, 40 kPa +load (anti-VE), and +thrombin, respectively.

4. Discussion

These findings reveal the coordinate impact of substrate stiffness and force-transduction signaling on endothelial cell contractility and gap formation. Matrix rigidity is well known to increase cell contractility and tension on cell-cell junctions [2,8,22,36]. However, perturbations such as mechanical stretch and fluid shear stress can activate intercellular force transduction signals that further increase contractility, and perturb both cell-cell and cell-matrix adhesions [3,4,18,52]. Using a combination of mechanical perturbations and both mechanical and biochemical readouts of cell responses, these findings demonstrate that substrate stiffness increases the amplitudes of stress variations within endothelial monolayers. This in turn enhances endothelial gap formation, in response to VE-cadherin dependent force-transduction signals. In a prior study of ECs on glass, VE-cadherin-activated signals increased cell contractility and disrupted junctions up to ~3 cell diameters from the site of stimulation [21]. The present studies show that substrate stiffness modulates this force-activated endothelial disruption. Furthermore, greater stress fluctuations in monolayers on stiffer substrates appear to predispose monolayers to inter-endothelial gap formation. Interestingly, our findings also suggest that, although force-transduction signals disrupt intercellular junctions, the effects appear to be localized such that the overall mechanical equilibrium is maintained at the mesoscale.

The relative adaptive stiffening activated by VE-cadherin perturbations was greater in EC colonies on soft gels relative to stiff hydrogels or glass substrates. The substrate-dependent differences could be explained by an upper bound to cell contractility. In this scenario, the lower basal prestress in cells on soft gels could increase the dynamic range of the mechanical response. Interestingly, on soft gels, despite the slightly greater increase in cell stiffening, the mechanical perturbations did not alter the RMS traction at the mesoscale (colony level).

Cadherin-mediated force transduction activates cell stiffening through an integrin dependent increase in myosin contractility [21,26]. On stiff hydrogels, but not on soft gels, force transduction triggered increases in both the sizes and numbers of focal adhesions in ECs. A prior study of epithelial cells reported changes in focal adhesion size and area in cells on both 40 kPa and 8.8 kPa hydrogels [26]. However, the present study used softer 1.1 kPa gels, and softer substrates are well known to reduce integrin activation and ligand binding [24,48,53]. But VE-cadherin-mediated force transduction activates phospho-inositide-3-kinase, which can result in integrin activation by inside-out signaling [26]. Kinase dependent integrin activation could thus increase contractility, independent of detectable FA remodeling and growth [18,21,49]. Moreover, a lower initial population of active integrins could also increase the dynamic range of integrin-mediated adaptive stiffening.

At the colony level, adaptive stiffening responses did not correlate with the measured RMS tractions. This might appear to contradict a prior finding that individual epithelial cells exhibited greater increases in RMS traction on stiff gels relative to soft ones, following cadherin-specific perturbations [26]. However, we attribute the apparent *decrease* in the *area-averaged* RMS traction in these endothelial monolayers to the increase in gap formation on stiff gels and consequent reduction in cell-substrate contact area.

The balance between cell-substrate tractions and intercellular tugging forces is postulated to determine the mechanical state of endothelial monolayers, in the absence of perturbations [8]. This force balancing was demonstrated with cell pairs [45,54], and a 'tissue model' validated force balancing within small cell clusters [39]. Our results show that stiffer substrates increase the basal RMS traction (at t = 0 s) (Fig. S.I. 3A), the basal NCM (Fig. S.I. 3B), and the basal interendothelial stress (Fig. S.I. 3C) in EC monolayers (Fig. S.I. 3C). Despite these global changes, VE-cadherin stimulation did not affect the monolayer-averaged shear and normal stresses, within experimental error.

The MSM heat maps of cells on stiff versus soft substrates do, however, correlate with the relative instability of interendothelial junctions within the monolayers. The maximum principal stresses (σ_{max}) and standard deviation were much smaller in monolayers on soft substrates, resulting in more uniform heat maps (Table 2 and Fig. 7). By contrast, on stiff hydrogels, large spatial variations in the amplitude of the σ_{max} vectors suggested regions of both highly stressed and relatively unstressed cell-cell contacts. The monolayers appear primed for destabilization, as might be predicted if

force instability presages gap formation in response to stimuli [9]. This postulate is borne out by the substantial monolayer disruption triggered by VE-cadherin perturbations in cells on stiff, but not on soft substrates.

It was surprising that VE-cadherin perturbations, which triggered the remodeling of both cell-cell and cell-matrix adhesions, did not trigger significant changes in the population average NCM or RMS tractions. By contrast, thrombin treatment, which is known to trigger massive endothelial disruption [2,8,36], stimulated major shifts in both the normalized NCM and σ_{ave} in the monolayer. Thrombin stimulation reflects an extreme perturbation, but the relative impact of intercellular (VE-cadherin) force-transduction on the global monolayer mechanics is much smaller. The changes also appear to be smaller than the large, intrinsic stress variations in the monolayer on stiff substrates. VE-cadherin-activated signals do locally disrupt the monolayers, but the effects appear to be more localized and to quickly dissipate, by redistributing forces between cell-matrix and cell-cell adhesions, without altering mesoscale tissue mechanics. In the context of tissue physiology, this more modest response would be expected for biochemical processes that facilitate cytoskeletal and tissue remodeling, as in the case of endothelial shear alignment [18] or junction reinforcement in cyclically stretched endothelium [3,4]. By contrast, inflammatory mediators such as thrombin trigger rapid, extensive changes in endothelial barriers [4,8,36].

Although these studies were done in the absence of flow, the findings are relevant to vascular endothelial function. Fluid shear stress alters the tension on VE-cadherin adhesions [18], and flow dependent force fluctuations at junctions activate signaling via a PECAM-1/VEGFR2/VE-cadherin 'complex', to regulate endothelial shear alignment [1,18]. Perturbing VE-cadherin receptors with VE-cadherin modified beads triggers the same force-transduction signaling cascade, and thereby mimics signals that regulate flow sensing. The vascular endothelium experiences location-dependent flow profiles and shear forces. In straight sections of the arterial tree, the wall shear stress is ~1.2 Pa (12 dyn/cm^2), which is atheroprotective [2,55]. However, at arterial tree bifurcations or in regions of high curvature, wall shear stresses can be as low as 0 Pa. Such regions can become sites of atherosclerotic plaque formation [56]. Our results thus suggest how arterial stiffening, for example, might alter endothelial responses to such variations in wall shear stresses or in regions of disturbed flow.

We expect that similar force-transduction signaling may also affect other mechanically-sensitive processes that regulate endothelial functions. For example, pathological levels of mechanical stretch, as in ventilator induced lung injury [7,57], activate kinase cascades via VE-cadherin and VEGFR2 to induce endothelial junction remodeling [20]. These findings might also predict that arterioles in fibrotic lung tissue would be more susceptible to damage by mechanical ventilation. Increased hydraulic pressure in hypertension also correlates with increased protein excretion in the kidney [58,59].

5. Conclusion

These results demonstrate the interplay between intercellular (VE-cadherin) force transduction signaling and matrix stiffness in regulating cell-cell and cell-matrix adhesions, as well as endothelial monolayer integrity. The range of substrate stiffness from 1.1 kPa to 40 kPa is within the range of stiffness variations measured *ex vivo* for lung arteries and parenchyma [17,60]. In this range, matrix stiffness increases both the average stress and the stress variations within endothelial monolayers. The latter appear to predispose monolayers to junction disruption in response to mechanical perturbations that could result, for example, from flow disturbances or

mechanical ventilation. Our findings also suggest how stiffening of the tunica intima due to age related turnover and deposition of extracellular matrix components [16] could contribute to endothelial junction destabilization, leading to increased permeability [36], atherogenesis [61], and perturbed blood flow [56].

Author contributions

R.C.A.E. designed and conducted experiments, analyzed and interpreted data, and wrote the manuscript. K.B.K. provided reagents, interpreted data, and assisted with writing of the manuscript. G.H.U. interpreted data and assisted with writing of the manuscript, D.E.L. designed experiments, interpreted data, and wrote the manuscript.

Acknowledgments

Appendix A. Supplementary data

Supplementary data related to this article can be found at http://dx.doi.org/10.1016/j.biomaterials.2017.06.010.

References

[1] E. Tzima, M. Irani-Tehrani, W.B. Kiosses, E. DeJana, D.A. Schultz, B. Engelhardt, G. Cao, H. DeLisser, M.A. Schwartz, A mechanosensory complex that mediates the endothelial cell response to fluid shear stress, Nature 437 (2005) 426—431, http://dx.doi.org/10.1038/Nature03952.

[2] J.C. Kohn, D.W. Zhou, F. Bordeleau, A.L. Zhou, B.N. Mason, M.J. Mitchell, M.R. King, C.A. Reinhart-King, Cooperative effects of matrix stiffness and fluid shear stress on endothelial cell behavior, Biophys. J. 108 (2015) 471—478, http://dx.doi.org/10.1016/j.bpj.2014.12.023.

[3] A.A. Birukova, S. Chatchavalvanich, A. Rios, K. Kawkitinarong, J.G.N. Garcia, K.G. Birukov, Differential regulation of pulmonary endothelial monolayer integrity by varying degrees of cyclic stretch, Am. J. Pathol. 168 (2006) 1749—1761, http://dx.doi.org/10.2353/ajpath.2006.050431.

[4] A. Dan, R.B. Huang, D.E. Leckband, Dynamic imaging reveals coordinate effects of cyclic stretch and substrate stiffness on endothelial integrity, Ann. Biomed. Eng. (2016) 1—13, http://dx.doi.org/10.1007/s10439-016-1677-4.

[5] P.M. Cummins, N.V.O. Sweeney, M.T. Killeen, Y.A. Birney, E.M. Redmond, P.A. Cahill, Cyclic strain-mediated matrix metalloproteinase regulation within the vascular endothelium?: a force to be reckoned with, Am. J. Physiol. Heart Circ. Physiol. 292 (2007) H28—H42, http://dx.doi.org/10.1152/ajpheart.00304.2006.

[6] A.A. Birukova, A. Rios, K.G. Birukov, Long-term cyclic stretch controls pulmonary endothelial permeability at translational and post-translational levels, Exp. Cell Res. 314 (2008) 3466—3477, http://dx.doi.org/10.1016/j.yexcr.2008.09.003.

[7] S.M. Dudek, J.G.N. Garcia, Cytoskeletal regulation of pulmonary vascular permeability, J. Appl. Physiol. 91 (2001) 1487—1500.

[8] R. Krishnan, D.D. Klumpers, C.Y. Park, K. Rajendran, X. Trepat, J. van Bezu, V.W.M. van Hinsbergh, C.V. Carman, J.D. Brain, J.J. Fredberg, J.P. Butler, G.P. van Nieuw Amerongen, Substrate stiffening promotes endothelial monolayer disruption through enhanced physical forces, Am. J. Physiol. Cell Physiol. 300 (2011) C146—C154, http://dx.doi.org/10.1152/ajpcell.00195.2010.

[9] E.T. Valent, G.P. van Nieuw Amerongen, V.W.M. van Hinsbergh, P.L. Hordijk, Traction force dynamics predict gap formation in activated endothelium, Exp. Cell Res. 347 (2016) 161—170, http://dx.doi.org/10.1016/j.yexcr.2016.07.029.

[10] J. Oldenburg, J. de Rooij, Mechanical control of the endothelial barrier, Cell Tissue Res. 355 (2014) 545—555, http://dx.doi.org/10.1007/s00441-013-1792-6.

[11] K.L. Mui, C.S. Chen, R.K. Assoian, The mechanical regulation of integrin-cadherin crosstalk organizes cells, signaling and forces, J. Cell Sci. (2016) 1—8, http://dx.doi.org/10.1242/jcs.183699.

[12] S. Chien, S. Li, J.Y.-J. Shyy, Effects of mechanical forces on signal transduction gene expression in endothelial, Hypertension 31 (1998) 162—169.

[13] B. Folkow, Physiological aspects of primary hypertension, Physiol. Rev. 62 (1982) 347—504.

[14] S.J. Zieman, V. Melenovsky, D.A. Kass, Mechanisms, pathophysiology, and therapy of arterial stiffness, Arterioscler. Thromb. Vasc. Biol. 25 (2005) 932–943, http://dx.doi.org/10.1161/01.ATV.0000160548.78317.29.

[15] M.M. Redfield, S.J. Jacobsen, B.A. Borlaug, R.J. Rodeheffer, D.A. Kass, Age- and gender-related ventricular-vascular stiffening: a community-based study, Circulation 112 (2005) 2254–2262, http://dx.doi.org/10.1161/CIRCULATIONAHA.105.541078.

[16] T.J.M. Schlatmann, A.E. Becker, Histologic changes in the normal aging aorta: implications for dissecting aortic aneurysm, Am. J. Cardiol. 39 (1977) 13–20, http://dx.doi.org/10.1016/S0002-9149(77)80004-0.

[17] J. Huynh, N. Nishimura, K. Rana, J.M. Peloquin, J.P. Califano, C.R. Montague, M.R. King, C.B. Schaffer, C. a. Reinhart-King, Age-related intimal stiffening enhances endothelial permeability and leukocyte transmigration, Sci. Transl. Med. 3 (2011) 112ra122, http://dx.doi.org/10.1126/scitranslmed.3002761.

[18] D.E. Conway, M.T. Breckenridge, E. Hinde, E. Gratton, C.S. Chen, M.A. Schwartz, Fluid shear stress on endothelial cells modulates mechanical tension across VE-cadherin and PECAM-1, Curr. Biol. 23 (2013) 1024–1030, http://dx.doi.org/10.1016/j.cub.2013.04.049.

[19] B.G. Coon, N. Baeyens, J. Han, M. Budatha, T.D. Ross, J.S. Fang, S. Yun, J.L. Thomas, M.A. Schwartz, Intramembrane binding of VE-cadherin to VEGFR2 and VEGFR3 assembles the endothelial mechanosensory complex, J. Cell Biol. 208 (2015) 975–986, http://dx.doi.org/10.1083/jcb.201408103.

[20] Y. Tian, G. Gawlak, J. O'Donnell, A.A. Birukova, K.G. Birukov, Activation of Vascular Endothelial Growth Factor (VEGF) receptor 2 mediates endothelial permeability caused by cyclic stretch, J. Biol. Chem. 291 (2016) 10032–10045, http://dx.doi.org/10.1074/jbc.M115.690487.

[21] A.K. Barry, N. Wang, D.E. Leckband, D.E. Leckband, C. Sciences, Local VE-cadherin mechanotransduction triggers long- ranged remodeling of endo-thelial monolayers, J. Cell Sci. 128 (2015) e0705.

[22] J.C. Kohn, M.C. Lampi, C.A. Reinhart-King, Age-related vascular stiffening: causes and consequences, Front. Genet. 6 (2015) 1–17, http://dx.doi.org/10.3389/fgene.2015.00112.

[23] M. Amano, M. Nakayama, K. Kaibuchi, Rho-kinase/ROCK: a key regulator of the cytoskeleton and cell polarity, Cytoskeleton 67 (2010) 545–554, http://dx.doi.org/10.1002/cm.20472.

[24] A. Elosegui-Artola, E. Bazellières, M.D. Allen, I. Andreu, R. Oria, R. Sunyer, J.J. Gomm, J.F. Marshall, J.L. Jones, X. Trepat, P. Roca-Cusachs, Rigidity sensing and adaptation through regulation of integrin types, Nat. Mater. 13 (2014) 631–637, http://dx.doi.org/10.1038/nmat3960.

[25] Y. Wang, G. Jin, H. Miao, J.Y.-S. Li, S. Usami, S. Chien, Integrins regulate VE-cadherin and catenins: dependence of this regulation on Src, but not on Ras, Proc. Natl. Acad. Sci. U. S. A. 103 (2006) 1774–1779, http://dx.doi.org/10.1073/pnas.0510774103.

[26] I. Muhamed, J. Wu, P. Sehgal, X. Kong, A. Tajik, N. Wang, D.E. Leckband, E-Cadherin-mediated force transduction signals regulate global cell mechanics, J. Cell Sci. (2016), http://dx.doi.org/10.1242/jcs.185447 jcs.185447-.

[27] A.K. Barry, N. Wang, D.E. Leckband, Local VE-cadherin mechanotransduction triggers long-ranged remodeling of endothelial monolayers, J. Cell Sci. 128 (2015) 1341–1351, http://dx.doi.org/10.1242/jcs.159954.

[28] J.P. Butler, I.M. Tolić-Nørrelykke, B. Fabry, J.J. Fredberg, Traction fields, mo-ments, and strain energy that cells exert on their surroundings, Am. J. Physiol. Cell Physiol. 282 (2002) C595–C605, http://dx.doi.org/10.1152/ajpcell.00270.2001.

[29] J.R. Tse, A.J. Engler, Preparation of hydrogel substrates with tunable me-chanical properties, Curr. Protoc. Cell Biol. (2010) 1–16, http://dx.doi.org/10.1002/0471143030.cb1016s47.

[30] C.J. Flaim, S. Chien, S.N. Bhatia, An extracellular matrix microarray for probing cellular differentiation, Nat. Methods 2 (2005) 119–125, http://dx.doi.org/10.1038/nmeth736.

[32] D.A. Brafman, S. Chien, K. Willert, Arrayed cellular microenvironments for identifying culture and differentiation conditions for stem, primary and rare cell populations, Nat. Protoc. 7 (2012) 703–717, http://dx.doi.org/10.1038/nprot.2012.017.

[33] H.-Y. Chiang, V.A. Korshunov, A. Serour, F. Shi, J. Sottile, Fibronectin is an important regulator of flow-induced vascular remodeling, Arterioscler. Thromb. Vasc. Biol. 29 (2009) 1074–1079, http://dx.doi.org/10.1161/ATVBAHA.108.181081.

[34] B. Fabry, G.N. Maksym, J.P. Butler, M. Glogauer, D. Navajas, J.J. Fredberg, Scaling the microrheology of living cells, Phys. Rev. Lett. 87 (2001) 1–4, http://dx.doi.org/10.1103/PhysRevLett.87.148102.

[35] B.E.N. Fabry, G.N. Maksym, S.A. Shore, P.E. Moore, R.A. Panettieri, J.P. Butler, J.J. Fredberg, G.N. Maksym, S.A. Shore, P.E. Moore, R.A. Panettieri, J.P. But, J.J. Fredberg, Signal transduction in smooth muscle selected contribution: time course and heterogeneity of contractile responses in cultured human airway smooth muscle cells, J. Appl. Physiol. 91 (2001) 986–994.

[36] A.A. Birukova, X. Tian, I. Cokic, Y. Beckham, M.L. Gardel, K.G. Birukov, Endo-thelial barrier disruption and recovery is controlled by substrate stiffness, Microvasc. Res. 87 (2013) 50–57, http://dx.doi.org/10.1016/j.mvr.2012.12.006.

[37] X. Trepat, M.R. Wasserman, T.E. Angelini, E. Millet, D.A. Weitz, J.P. Butler, J.J. Fredberg, Physical forces during collective cell migration, Nat. Phys. 5 (2009) 426–430, http://dx.doi.org/10.1038/nphys1269.

[38] D.T. Tambe, U. Croutelle, X. Trepat, C.Y. Park, J.H. Kim, E. Millet, J.P. Butler, J.J. Fredberg, Monolayer stress microscopy: limitations, artifacts, and accuracy of recovered intercellular stresses, PLoS One 8 (2013) e55172, http://dx.doi.org/10.1371/journal.pone.0055172.

[39] M.R. Ng, A. Besser, J.S. Brugge, G. Danuser, Mapping the dynamics of force transduction at cell-cell junctions of epithelial clusters, Elife 4 (2014) e03282, http://dx.doi.org/10.7554/eLife.03282.

[40] E. Zamir, B.Z. Katz, S. Aota, K.M. Yamada, B. Geiger, Z. Kam, Molecular diversity of cell-matrix adhesions, J. Cell Sci. 112 (pt11) (1999) 1655–1669.

[41] E.M. Gonon, M. Skalski, M. Kean, M.G. Coppolino, SNARE-mediated membrane traffic modulates RhoA-regulated focal adhesion formation, FEBS Lett. 579 (2005) 6169–6178, http://dx.doi.org/10.1016/j.febslet.2005.09.090.

[42] S. Huveneers, J. Oldenburg, E. Spanjaard, G. van der Krogt, I. Grigoriev, A. Akhmanova, H. Rehmann, J. de Rooij, Vinculin associates with endothelial VE-cadherin junctions to control force-dependent remodeling, J. Cell Biol. 196 (2012) 641–652, http://dx.doi.org/10.1083/jcb.201108120.

[43] N. Wang, I.M. Tolić-Nørrelykke, J. Chen, S.M. Mijailovich, J.P. Butler, J.J. Fredberg, D. Stamenović, Cell prestress. I. Stiffness and prestress are closely associated in adherent contractile cells, Am. J. Physiol. Cell Physiol. 282 (2002) C606–C616, http://dx.doi.org/10.1152/ajpcell.00269.2001.

[44] T.-J. Kim, S. Zheng, J. Sun, I. Muhamed, J. Wu, L. Lei, X. Kong, D.E. Leckband, Y. Wang, Dynamic visualization of α-catenin reveals rapid, reversible conformation switching between tension states, Curr. Biol. 25 (2015) 218–224, http://dx.doi.org/10.1016/j.cub.2014.11.017.

[45] V. Maruthamuthu, B. Sabass, U.S. Schwarz, M.L. Gardel, Cell-ECM traction force modulates endogenous tension at cell-cell contacts, Proc. Natl. Acad. Sci. U. S. A. 108 (2011) 4708–4713, http://dx.doi.org/10.1073/pnas.1011123108.

[46] M.A. Schwartz, D.W. DeSimone, Cell adhesion receptors in mechano-transduction, Curr. Opin. Cell Biol. 20 (2008) 551–556, http://dx.doi.org/10.1016/j.ceb.2008.05.005.

[47] Q. Le Duc, Q. Shi, I. Blonk, A. Sonnenberg, N. Wang, D. Leckband, J. De Rooij, Vinculin potentiates E-cadherin mechanosensing and is recruited to actin-anchored sites within adherens junctions in a myosin II-dependent manner, J. Cell Biol. 189 (2010) 1107–1115, http://dx.doi.org/10.1083/jcb.201001149.

[48] A. Elosegui-Artola, R. Oria, Y. Chen, A. Kosmalska, C. Pérez-González, N. Castro, C. Zhu, X. Trepat, P. Roca-Cusachs, Mechanical regulation of a molecular clutch defines force transmission and transduction in response to matrix rigidity, Nat. Cell Biol. 18 (2016) 540–548, http://dx.doi.org/10.1038/ncb3336.

[49] C. Collins, C. Guilluy, C. Welch, E.T. O'Brien, K. Hahn, R. Superfine, K. Burridge, E. Tzima, Localized tensional forces on PECAM-1 elicit a global mechano-transduction response via the integrin-RhoA pathway, Curr. Biol. 22 (2012) 2087–2094, http://dx.doi.org/10.1016/j.cub.2012.08.051.

[50] S. Banerjee, M.C. Marchetti, Contractile stresses in cohesive cell layers on finite-thickness substrates, Phys. Rev. Lett. 109 (2012) 1–5, http://dx.doi.org/10.1103/PhysRevLett.109.108101.

[51] T. Yeung, P.C. Georges, L.A. Flanagan, B. Marg, M. Ortiz, M. Funaki, N. Zahir, W. Ming, V. Weaver, P.A. Janmey, Effects of substrate stiffness on cell morphology, cytoskeletal structure, and adhesion, cell Motil, Cytoskeleton 60 (2005) 24–34, http://dx.doi.org/10.1002/cm.20041.

[52] C. Wang, B.M. Baker, C.S. Chen, M.A. Schwartz, Endothelial cell sensing of flow direction, Arterioscler. Thromb. Vasc. Biol. 33 (2013) 2130–2136, http://dx.doi.org/10.1161/ATVBAHA.113.301826.

[53] Z. Rahil, S. Pedron, X. Wang, T. Ha, B. Harley, D. Leckband, Nanoscale me-chanics guides cellular decision making, Integr. Biol. 8 (2016) 929–935, http://dx.doi.org/10.1039/C6IB00113K.

[54] Z. Liu, J.L. Tan, D.M. Cohen, M.T. Yang, N.J. Sniadecki, S.A. Ruiz, C.M. Nelson, C.S. Chen, Mechanical tugging force regulates the size of cell-cell junctions, Proc. Natl. Acad. Sci. 107 (2010) 9944–9949, http://dx.doi.org/10.1073/pnas.0914547107.

[55] S.S. Hur, Y. Zhao, Y.S. Li, E. Botvinick, S. Chien, Live cells exert 3-dimensional traction forces on their substrata, Cell. Mol. Bioeng. 2 (2009) 425–436, http://dx.doi.org/10.1007/s12195-009-0082-6.

[56] J.-J. Chiu, S. Chien, Effects of disturbed flow on vascular endothelium: path-ophysiological basis and clinical perspectives, Physiol. Rev. 91 (2011) 327–387, http://dx.doi.org/10.1152/physrev.00047.2009.

[57] F.R. Millar, C. Summers, M.J. Griffiths, M.R. Toshner, A.G. Proudfoot, The pul-monary endothelium in acute respiratory distress syndrome: insights and therapeutic opportunities, Thorax 71 (2016) 462–473, http://dx.doi.org/10.1136/thoraxjnl-2015-207461.

[58] M.R. Weir, Hypertension and the kidney: perspectives on the relationship of kidney disease and cardiovascular disease, Clin. J. Am. Soc. Nephrol. 4 (2009) 2045–2050, http://dx.doi.org/10.2215/CJN.03050509.

[59] B.I. Freedman, J.R. Sedor, Hypertension-associated kidney disease: perhaps no more, J. Am. Soc. Nephrol. 19 (2008) 2047–2051, http://dx.doi.org/10.1681/ASN.2008060621.

[60] F. Liu, J.D. Mih, B.S. Shea, A.T. Kho, A.S. Sharif, A.M. Tager, D.J. Tschumperlin, Feedback amplification of fibrosis through matrix stiffening and COX-2 sup-pression, J. Cell Biol. 190 (2010) 693–706, http://dx.doi.org/10.1083/jcb.201004082.

[61] R. Ross, L. Agius, The process of atherogenesis m cellular and molecular interaction: from experimental animal models to humans, Diabetologia 100 (1992) 34–40.